Effect of Substituents on the Strength of Hypervalent Phosphorus−Halogen Bonds

Catherine E. Check, Kim C. Lobring, Pamela R. Keating, Thomas M. Gilbert,* and Lee S. Sunderlin*

Department of Chemistry and Biochemistry, Northern Illinois University, DeKalb, Illinois 60115

Received: February 28, 2003; In Final Form: July 11, 2003

The strengths of the $F_2ClP-Cl^-$, $POCl_3-Cl^-$, and $PSCl_3-Cl^-$ bonds have been determined by measuring thresholds for collision-induced dissociation in a flowing afterglow-tandem mass spectrometer. The results are combined with previously determined values for the PF_4^-, PF_3Cl^-, POF_4^-, and PCl_4^- systems to determine the effect of adjacent ligands on hypervalent bond strengths. Although the addition of electronegative equatorial ligands strengthens bonding to axial halides, the effect is, in some cases, outweighed by the rearrangement energy of the dissociation products. Computational results indicate that the B3LYP/aug-cc-pVTZ method gives particularly good agreement with experiment among the models used here; however, several less resource-intensive methods give acceptable agreement.

Introduction

Although the phosphorus trihalide molecules PX_3 (where X = F, Cl, Br, and I) satisfy the octet rule, these molecules can act as electron-pair acceptors to form the corresponding tetrahalide anions PX_4^-. These anions are hypervalent,[1−8] because their electron dot structures show 10 electrons around the P atom. The X_3P-X^- bond strengths have now been measured in the gas phase for all four halogens,[9−11] and several bond strengths in 15 mixed-group tetrahalides are also known. There is a linear correlation between the bond strengths and the difference in the electronegativities of the central atom and the halogen. However, the X_3P-X^- bond strengths also reflect the influence of the axial P−X bond trans to the broken bond, as well as the two equatorial P−X bonds. Furthermore, electronegativity correlates with many other properties, including electron affinities, atomic sizes, and dipole moments. Thus, it is difficult to say which factors have a major influence on the bond strength.

One approach to determine the influences on bond strengths is to compare molecules where several factors are the same. For example, $PF_2Cl_2^-$ is similar to PCl_4^-, except that two of the Cl atoms have been replaced by F atoms, and PEX_4^- (where E = O or S) can be considered to be a PX_4^- molecule where the lone pair on the P atom has been replaced by an oxide or sulfide, as shown in Figure 1. Differences between the $P-X^-$ bond strengths in these systems must be due to the effects of the substituents, although it is important to note that the substituents affect both the PX_4^- or PEX_4^- reactants and the PX_3 or PEX_3 halogen loss products. This work describes measurements of P−X bond strengths in $PF_2Cl_2^-$, $POCl_4^-$, and $PSCl_4^-$ and compares the results to recent data for PCl_4^- as well as literature values for PF_4^-, PF_3Cl^-, and POF_4^-. The experiments are conducted in the gas phase, to eliminate the effects of solvation on the bonding.[12]

A related study of halide anion affinities of main-group fluorides, oxyfluorides, and fluoride sulfides was performed by Larson and McMahon.[13] This work concentrated on periodic trends in isoelectronic series (such as F_3PO, F_2SO_2, and $FClO_3$); however, some results directly relate to this paper. Larson and McMahon previously reported a bond strength of $D(F_3P-F^-)$ = 168 kJ/mol. This value, which comes from a fluoride affinity scale that is based on a series of measurements of relative bond energies, should be adjusted to ca. 200 kJ/mol, because of changes in the scale.[14−16] The bond energy in POF_4^- was measured to be 32 kJ/mol higher than that in PF_4^-, and this relative number is unaffected by difficulties with the overall scale. The values $D(PF_3-Cl^-)$ = 65 kJ/mol[9] and $D(PCl_3-Cl^-)$ = 90 kJ/mol[11] have also been reported.

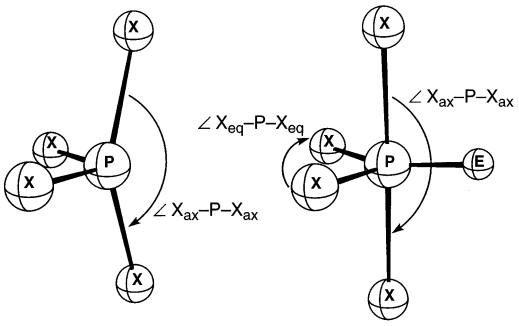

Figure 1. Geometrical parameters for molecules.

Two studies have reported computational results for POF_4^-.[17,18] Computational results for the other anions studied experimentally for this paper are lacking. However, a substantial amount of theoretical work on the nature of P−O and P−S bonding[19−22] and hypervalent phosphorus−halogen bonding has been performed.[1−8]

Methods

Bond strengths were measured using the energy-resolved collision-induced dissociation (CID) technique[23,24] in a flowing afterglow-tandem mass spectrometer (MS).[25] The instrument consists of an ion-source region, a flow tube, and the tandem MS. The dc discharge ion source used in these experiments is typically set at 2000 V with 2 mA of emission current. The flow tube is a stainless-steel pipe (92 cm long, inside diameter of 7.3 cm) that operates at a buffer gas pressure of 0.35 Torr,

* Authors to whom correspondence should be addressed. E-mail: sunder@niu.edu. E-mail: tgilbert@marilyn.chem.niu.edu.

10.1021/jp030287x CCC: $25.00
Published on Web 09/26/2003

a flow rate of 200 standard cm^3/s, and an ion residence time of 100 ms. The buffer gas is helium with up to 10% argon added, to stabilize the dc discharge.

To make $POCl_4^-$ for this study, $POCl_3$ was added to the ion source. Direct electron impact on $POCl_3$ has been studied previously, and the main products observed are $POCl_2^-$, $POCl_3^-$, and a small amount of Cl^-.[26] The main ion produced under our experimental conditions is $POCl_3^-$. Therefore, CCl_4 was added on some occasions as an additional Cl^- source. Cl^- is added to $POCl_3$ to form $POCl_4^-$; other plasma reactions also contribute to the population of this ion. Approximately 10^5 collisions with the buffer gas cool the metastable ions to room temperature.

$PSCl_4^-$ was made by adding $PSCl_3$ to the ion source, and $PF_2Cl_2^-$ was produced by adding PCl_3 and SF_6 to the ion source. All these ions were easier to produce than $POCl_4^-$, which suggests greater thermodynamic stability.

The tandem MS includes a quadrupole mass filter, an octopole ion guide, a second quadrupole mass filter, and a detector, contained in a stainless-steel box that is partitioned into five interior chambers. Differential pumping on the five chambers ensures that further collisions of the ions with the buffer gas are unlikely after ion extraction. During CID experiments, the ions are extracted from the flow tube and focused into the first quadrupole for mass selection. The reactant ions are then focused into the octopole, which passes through a reaction cell that contains a collision gas (argon in the present experiments). After the dissociated and unreacted ions pass through the reaction cell, the second quadrupole is used for mass analysis. The detector is an electron multiplier operating in pulse-counting mode.

The energy threshold for CID is determined by modeling the cross section for product formation as a function of the reactant-ion kinetic energy in the center-of-mass (CM) frame (E_{cm}). The octopole is used as a retarding field analyzer to measure the energy zero of the reactant ion beam. The kinetic energy distribution of the ion for the present data is typically Gaussian, with an average full-width at half-maximum of 0.8−1.1 eV (1 eV = 96.5 kJ/mol). The octopole offset voltage, which was measured with respect to the center of the Gaussian fit, gives the laboratory kinetic energy (E_{lab}, in electron volts). Low offset energies are corrected for truncation of the ion beam.[27] To convert to the CM frame, the equation $E_{cm} = E_{lab}m/(m + M)$ is used, where m and M are the masses of the neutral and ionic reactants, respectively. All experiments were performed with both mass filters at low resolution, to improve the ion collection efficiency and reduce mass discrimination. Average atomic masses were used for all elements.

The total cross section for a reaction, σ_{total}, is calculated using eq 1,

$$I = I_0 \exp(-\sigma_{total} n l) \tag{1}$$

where I is the intensity of the reactant ion beam, I_0 the intensity of the incoming beam ($I_0 = I + \Sigma I_i$), I_i the intensity of each product ion, n the number density of the collision gas, and l the effective collision length ($l = 13 \pm 2$ cm). Individual product cross sections σ_i are equal to $\sigma_{total}(I_i/\Sigma I_i)$.

Threshold energies are derived by fitting the data to a model function given in eq 2,

$$\sigma(E) = \sigma_0 \sum_i \frac{g_i(E + E_i - E_T)^n}{E} \tag{2}$$

where $\sigma(E)$ is the cross section for formation of the product ion at the CM energy E, E_T is the desired threshold energy, σ_0 is the scaling factor, n is an adjustable parameter, and i denotes rovibrational states that have an energy E_i and population g_i ($\Sigma g_i = 1$). Doppler broadening and the kinetic energy distribution of the reactant ion are also considered in the data analysis, which is done using the CRUNCH program that was written by P. B. Armentrout and co-workers.[27]

TABLE 1: Vibrational Frequencies and Rotational Constants

Vibrational Frequency (cm^{-1})		rotational	polarizability
experimental[a]	calculated[b]	frequency (cm^{-1})[b]	(10^{-24} cm^3)[b]
	$PF_2Cl_2^-$		
	100	0.0408	9.66
	139	0.0533	
	168	0.1017	
	234		
	264		
	384		
	448		
	562		
	752		
	PF_2Cl		
260	239	0.093	6.50
302	278	0.119	
411	382	0.241	
545	505		
852	785		
864	803		
	$POCl_4^-$		
	89.6	0.0347	13.48
	135	0.0424	
	189	0.0615	
	226		
	234		
	243		
	249		
	271		
	370		
	391		
	489		
	1224		
	$POCl_3$		
193	183 (2)	0.0467	8.93
267	259	0.0643	
337	320 (2)	0.0643	
486	444		
581	553 (2)		
1290	1299		
	$PSCl_4^-$		
	89.3	0.0280	16.90
	110	0.0285	
	168	0.0379	
	205		
	223		
	226		
	229		
	236		
	274		
	337		
	443		
	636		
	$PSCl_3$		
167	165 (2)	0.0442	11.81
250	237 (2)	0.0442	
250	246	0.0469	
435	398		
542	495 (2)		
753	732		

[a] From ref 28. [b] From present work, calculated at the B3LYP/6-311+G(d) level. Numbers in parentheses are degeneracies.

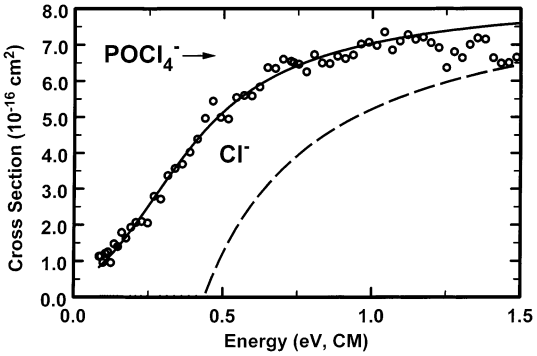

Figure 2. Cross section for the collision-induced dissociation (CID) of $POCl_4^-$, as a function of energy in the center-of-mass (CM) frame. Solid and dashed lines represent convoluted and unconvoluted fits to the data, respectively, as discussed in the text.

Experimental vibrational frequencies are not available for the anions studied in this work, although frequencies are available for the neutral dissociation products.[28−30] Therefore, vibrational and rotational frequencies were calculated using the B3LYP/6-311+G(d) model, to give a consistent set of frequencies, as given in Table 1. The calculated neutral frequencies are less than the known experimental values by 5% ± 3%, which is a typical result for this type of system.[31] Recent work on closely related molecules with the 6-311+G(d, p) and aug-cc-pVTZ basis sets suggests that both basis sets give generally good agreement with experiment without scaling.[32] Uncertainties in the derived thresholds due to possible inaccuracies in the frequencies were estimated by multiplying the entire sets of frequencies by factors of 0.9 and 1.1. The resulting changes in internal energies are <1 kJ/mol. Therefore, the calculated frequencies were used without scaling. Polarizabilities for neutral molecules were also taken from the computational results; varying these parameters has a negligible effect on the derived bond strengths.

Collisionally activated metastable complexes can have sufficiently long lifetimes that they do not dissociate on the experimental time scale (ca. 50 μs). Such kinetic shifts are considered in the CRUNCH program by Rice−Ramsperger−Kassel−Marcus (RRKM) lifetime calculations. The relatively small molecules studied in this work have small kinetic shifts (<0.2 kJ/mol). The uncertainty in the derived thresholds is again estimated by multiplying reactant or product frequency sets by factors of 0.9 and 1.1, and by multiplying the time window for dissociation by factors of 10 and 0.1. The effect of these variations is <1 kJ/mol; the main cause is the change in the calculated reactant internal energy content.

An ion that has not been sufficiently energized by one collision with the target gas may gain enough energy in a second collision to be above the dissociation threshold. This effect is eliminated by linear extrapolation of the data taken at several pressures to a zero-pressure cross section before fitting the data.[33]

The reagents $POCl_3$, $PSCl_3$, PCl_3, and CCl_4 were obtained from Aldrich. Helium, argon, and SF_6 were obtained from BOC. All reagents were used as received.

Computational work on these systems was performed using the Gaussian 98 Suite.[34] The Natural Bond Orbitals (NBO)[35] program was also used to study the charge distributions (natural population analysis) in these systems.

Results

CID of $POCl_4^-$ gives the loss of Cl^- (reaction 3) as the predominant product. $POCl_3^-$ and $POCl_2^-$ were also observed (reactions 4 and 5) but in quantities too small to measure effectively. Appearance curves for CID of $POCl_4^-$ are shown in Figure 2.

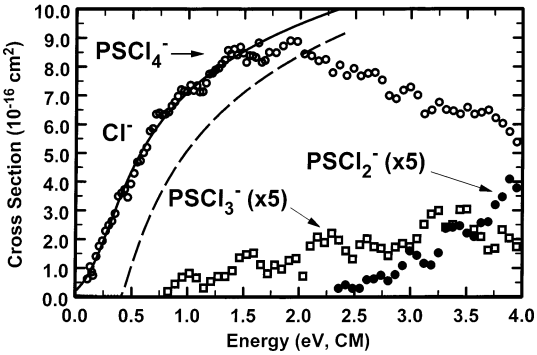

Figure 3. Cross section for the CID of $PSCl_4^-$, as a function of energy in the CM frame. Solid and dashed lines represent convoluted and unconvoluted fits to the data, respectively, as discussed in the text.

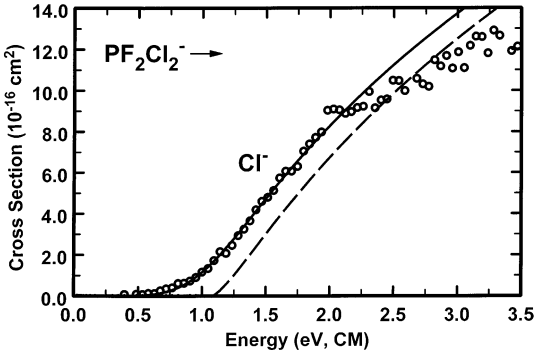

Figure 4. Cross section for the CID of $PF_2Cl_2^-$, as a function of energy in the CM frame. Solid and dashed lines represent convoluted and unconvoluted fits to the data, respectively, as discussed in the text.

$$POCl_4^- \rightarrow POCl_3 + Cl^- \quad (3)$$

$$POCl_4^- \rightarrow POCl_3^- + Cl \quad (4)$$

$$POCl_4^- \rightarrow POCl_2^- + Cl_2 \quad (5)$$

CID of $PSCl_4^-$ gives the loss of Cl^- (reaction 6) as the predominant product. $PSCl_3^-$, $PSCl_2^-$, and Cl_2^- (reactions 7, 8, and 9) were observed as the minor products, although Cl_2^- was detected in quantities too small to measure effectively. Appearance curves for CID of $PSCl_4^-$ are shown in Figure 3.

$$PSCl_4^- \rightarrow PSCl_3 + Cl^- \quad (6)$$

$$PSCl_4^- \rightarrow PSCl_3^- + Cl \quad (7)$$

$$PSCl_4^- \rightarrow PSCl_2^- + Cl_2 \quad (8)$$

$$PSCl_4^- \rightarrow PSCl_2 + Cl_2^- \quad (9)$$

CID of $PF_2Cl_2^-$ gives the loss of Cl^- (reaction 10) as the only observed product.

$$PF_2Cl_2^- \rightarrow PF_2Cl + Cl^- \quad (10)$$

The appearance curve for this anion is shown in Figure 4.

The fitting parameters in eq 2 for all three systems are given in Table 2, and the fits are also shown in Figures 2−4. The cross sections for minor products are negligible in the threshold region and are not included in the fit. The effects of reactant

TABLE 2: Fitting Parameters for CID[a]

anion	E_T (eV)	n
$POCl_4^-$	0.44 ± 0.05	0.9 ± 0.1
$PSCl_4^-$	0.43 ± 0.04	1.2 ± 0.1
$PF_2Cl_2^-$	1.03 ± 0.09	1.2 ± 0.1

[a] See text for a discussion of fitting parameters.

and product internal energy are included in the fitting procedure; therefore, the dissociation thresholds correspond to bond energies at 0 K. The final uncertainties in the bond energies are derived from the standard deviation of the thresholds determined for individual data sets, the uncertainty in the reactant internal energy, the effects of kinetic shifts, and the uncertainty in the energy scale (±0.15 eV lab). These results are given in Table 3.

The experimental bond energies at 0 K determined this way can be converted to bond enthalpies at 298 K using the integrated heat capacities of the reactants and products. The heat capacities were determined using the frequencies calculated at the B3LYP/6-311+G(d) level (see Table 1). These give bond enthalpies at 298 K that are almost identical (see Table 3).

Calculations on the molecules relevant to this study were performed using several models and basis sets. The optimized geometries are not very dependent on the basis set chosen. The geometries calculated using the B3LYP method and the largest basis set, aug-cc-pVTZ, are given in Table 4. Bond energies calculated with various methods using several basis sets are given in Table 3. NBO atomic charges are given in Table 5.

Discussion

Computed Geometries. All the anions studied in this work have five electron clouds (bonds or lone pairs) around the central P atom. The oxygen- and sulfur-containing species are distorted trigonal bipyramids, whereas the tetrahalides have disphenoidal geometries. Two electron clouds (ligands or a lone pair) are in axial (apical) locations, and three are equatorial. This is unlike the geometries for 8- or 12-electron systems, in that there are two distinct positions. When comparing bond strengths, it is important to determine whether the bonds are to axial or equatorial ligands. Normally, more-electronegative ligands are apicophilic;[36−39] more electropositive ligands prefer equatorial positions. Lone pairs can be considered to be directed toward empty space with an electronegativity of zero, and the PX_4^- systems all have the phosphorus lone pair in an equatorial position.

Anionic systems with mixed halogens apparently are exceptions to the general rule. For example, B3LYP/6-31+G(d) calculations[40] indicate that the isomer of SF_2Cl_2 with the F atoms in the axial positions is more stable than the isomer with the F atoms in the equatorial positions, by 9 kJ/mol. In the isoelectronic system $PF_2Cl_2^-$, we calculate, at the B3LYP/6-311+G(d) level, that the isomer with two *chlorine* ligands in the axial positions is lower in energy than the isomer with axial F atoms, by 80 kJ/mol. Calculations discussed below indicate that the $PF_2Cl_2^-$ isomer with axial F atoms has very large negative charges on the F atoms, whereas the structure with equatorial F atoms has a more-even charge distribution. The inversion of the apicophilicity trend for the anion is consistent with the more-even charge distribution, leading to greater stability. The most stable isomer of PF_3Cl^- also has the Cl atom in an axial position.

The $P-Cl_{ax}$ bond lengths in PCl_4^- and $PF_2Cl_2^-$ are essentially equal, and the $P-F_{eq}$ bond length in $PF_2Cl_2^-$ is shorter than that in PF_4^- by only 0.03 Å. The $X_{ax}-P-X_{ax}$ bond angle in $PF_2Cl_2^-$ lies between the angles for PCl_4^- and PF_4^-. Also, the P−F and P−Cl bond lengths in PF_3, PF_2Cl, and PCl_3 are almost identical. The similar geometries mean that comparison of bond strengths in these systems is reasonable. In contrast, the P−Cl bond is calculated to be 0.26 Å longer in PF_3Cl^- than in $PF_2Cl_2^-$, whereas the $P-F_{ax}$ bond in PF_3Cl^- is 0.10 Å shorter than that in PF_4^-, which indicates unequal sharing of the bonding electrons.

POF_4^-, $POCl_4^-$, and $PSCl_4^-$ are calculated to have the chalcogens in the equatorial position, regardless of the electronegativities. Axial bonds have a tendency to be longer than equatorial bonds. The shorter equatorial bond lengths are a better match for the chalcogens, because there is partial double-bond character to the P−O and P−S bonds. Thus, the bond energies measured in these experiments are for loss of *axial* halogen anions and are, therefore, comparable to the bond energies for PX_4^- systems.

The axial bond lengths in $POCl_4^-$ are 0.13 Å shorter than those in PCl_4^-, whereas the equatorial bond lengths are the same. For PF_4^-, the addition of an O atom is calculated to shorten the axial and equatorial P−F bond lengths, by 0.10 and 0.02 Å, respectively. The axial Cl−P−Cl bond angles in PCl_4^- and $POCl_4^-$ are 171° and 190°, which are similar to the ideal value of 180°. The corresponding F−P−F angles are somewhat larger, at 189° and 197°, which is consistent with the smaller steric influence of fluorine ligands compared to chlorine ligands. The $O-P-F_{ax}$ angle increases by 18.6° and the $O-P-F_{eq}$ angle decreases by 6.1° when an axial F atom is lost from POF_4^-. The corresponding changes in O−P−Cl angles during the dissociation of $POCl_4^-$ are slightly larger, at 19.9° and 9.5°.

TABLE 3: Computational Models and Energies for Halide Anion Dissociation from the Listed Anions

	PF_4^-	PF_3Cl^-	$PF_2Cl_2^-$	PCl_4^-	POF_4^-	$POCl_4^-$	$PSCl_4^-$
B3LYP/LANL2DZpd	211	82	114	110	254	56	44
B3LYP/6-31+G(d)	204	70	107	104	243	37	29
MP2(fc)/6-31+G(d)	199	71	97	88	240	31	24
MP2(fu)/6-31+G(d)	200	72	98	90	242	33	26
B3LYP/6-311+G(d)	209	75	111	108	243	42	33
MP2(fc)/6-311+G(d)	193	70	101	93	230	36	29
MP2(fu)/6-311+G(d)	194	71	102	94	231	37	30
G2(MP2)	197	64	100	103	239	32	49
B3LYP/aug-cc-pVTZ	190	64	103	98	228	40	32
experiment, 0 K	200	**65** ± 8	99 ± 9	90 ± 7	233	43± 5	41 ± 4
experiment, 298 K	200	**65** ± 8[a]	99 ± 9	90 ± 7	232[a]	43 ± 5	41 ± 4
No Zero Point Energy Corrections							
B3LYP/aug-cc-pVTZ	193	65	103	97	233	40	31
Snap Energies							
B3LYP/aug-cc-pVTZ	261	86	167	158	441	222	190

TABLE 4: Predicted (B3LYP/aug-cc-pVTZ level) and Experimental Structural Data for $PF_{3-x}Cl_x$ (x = 0, 1, 3), $PF_{4-x}Cl_x^-$ (x = 0, 1, 2, 4), $POX_3/PSCl_3$, and $POX_4^-/PSCl_4^-$ (X = F, Cl)[a]

	P−F (Å)	P−Cl (Å)	X−P−X (deg)	F−P−Cl (deg)
PF_3	1.591		97.4	
exp (ED)[b]	1.570 (1)		97.8 (2)	
exp (MW)[c]	1.561 (1)		97.7 (2)	
PF_2Cl	1.595	2.077	97.2	98.9
exp (MW)[d]	1.571 (3)	2.030 (6)	97.3 (2)	99.2 (2)
PCl_3		2.082	100.7	
exp (ED)[e]		2.039 (1)	100.27 (9)	
exp (MW)[f]		2.043 (3)	100.1 (3)	

	P−X_{ax} (Å)	P−X_{eq} (Å)	X_{eq}−P−X_{ax} (deg)	X_{eq}−P−X_{eq} (deg)	X_{ax}−P−X_{ax} (deg)
PF_4^-	1.780	1.635	87.1	99.0	189.1
PF_3Cl^-	1.685 (F), 2.686 (Cl)	1.609	91.4 (F−P−F), 86.9 (F−P−Cl)	97.9	182.6
$PF_2Cl_2^-$	2.424	1.605	90.1	97.7	179.8
PCl_4^-	2.429	2.118	92.8	100.1	171.2

	P−O(S) (Å)	P−X (Å)	O(S)−P−X (deg)	X−P−X (deg)
POF_3	1.449	1.548	117.2	100.7
exp (MW)[g]	1.45 (3)	1.52 (2)		102.5 (2)
$POCl_3$	1.464	2.032	114.8	103.6
exp (MW)[h]	1.4464 (2)	1.9929 (2)	114.91 (2)	103.53
$PSCl_3$	1.907	2.052	116.4	101.8
exp (MW)[g]	1.85 (2)	2.02 (1)		100.5 (1)

	P−O(S) (Å)	P−X_{ax} (Å)	P−X_{eq} (Å)	O(S)−P−X_{ax} (deg)	O(S)−P−X_{eq} (deg)	X_{eq}−P−X_{ax} (deg)	X_{eq}−P−X_{eq} (deg)	X_{ax}−P−X_{ax} (deg)
POF_4^-	1.485	1.681	1.614	98.6	123.3	85.3	113.5	197.2
$POCl_4^-$	1.480	2.302	2.114	94.9	124.3	87.3	111.5	189.7
$PSCl_4^-$	1.960	2.319	2.119	96.2	124.7	86.5	110.6	192.5

[a] Subscripts eq and ax represent equatorial and axial, respectively. ED = electron diffraction study, MW = microwave study. [b] From ref 47. [c] From ref 48. [d] From ref 49. [e] From ref 50. [f] From ref 51. [g] From ref 52. [h] From ref 53.

TABLE 5: Calculated Atomic Charges Using B3LYP/6-311+G(d) and the NBO Method

molecule	q_P	q_X axial	q_X equatorial	$q_{O/S}$
PF_4^-	1.59	−0.70	−0.60	
PCl_4^-	0.79	−0.58	−0.32	
$PF_2Cl_2^-$	1.44	−0.63	−0.59	
PF_3Cl^-	1.62	−0.65 F, −0.80 Cl	−0.59	
POF_4^-	2.52	−0.58	−0.63	−1.11
$POCl_4^-$	1.49	−0.47	−0.27	−1.01
$PSCl_4^-$	0.86	−0.46	−0.25	−0.43

A metastable $POCl_3$−Cl^- complex with a 3-fold symmetry axis and a P−Cl^- bond length of 3.98 Å is also predicted by the computational results. This is too far for significant covalent bonding; instead, the Cl atom aligns with the dipole moment of an almost-tetrahedral $POCl_3$ molecule, and ion−dipole and ion-induced dipole forces hold the complex together. The NBO charge [B3LYP/6-311+G(d)] on the weakly bound Cl atom (−0.99) is consistent with that of a slightly perturbed Cl^- anion. The P-atom charge of +1.55 and the O-atom charge of −1.02 are consistent with a P^+−O^- single bond, with minor contributions from other resonance structures. The energy of this structure is 10 kJ/mol greater than that of the disphenoidal structure at the B3LYP/6-311+G(d) level of theory, which suggests that it is thermodynamically unstable under the conditions of the flow tube. There is no evidence for its existence in our experiments.

Theoretical and Experimental Bond Energies. Several trends are apparent in the calculated bond strengths. The B3LYP/LANL2DZpd calculations use the LANL2DZ basis set, which has a frozen core and a double-ζ valence basis set,[41] supplemented by polarization and diffuse functions. This basis set gives bond strengths that are all greater than experimental values, by an average of 14 ± 6 kJ/mol. The B3LYP method gives better results with the 6-31+G(d), 6-311+G(d), and aug-cc-pVTZ basis sets; average absolute differences between calculations and experiment are 8 ± 4, 10 ± 5, and 5 ± 4 kJ/mol, respectively. The 6-31+G(d) and 6-311+G(d) results are generally greater than the experimental results, whereas the aug-cc-pVTZ results are generally less.

The MP2(full) calculations with the 6-31+G(d) and 6-311+G(d) basis sets give average absolute deviations from the experimental values of 6 ± 6 and 5 ± 3 kJ/mol, respectively. MP2(fc) calculations, where core electrons are frozen during the perturbation portion of the calculation, give bond energies that are consistently1−2 kJ/mol less than those obtained from MP2(full) with both of these basis sets.

The G2(MP2) method uses an extensive set of corrections to estimate the final energy that would be determined by a very high-level ab initio calculation. The average absolute deviation for this method is 6 ± 5 kJ/mol. Thus, all computational methods used, except the frozen core method B3LYP/LANL2DZpd (which will not be considered further), give results that, on average, differ from the experimental results by no more than the experimental uncertainties of 4−10 kJ/mol.

Comparison of PCl_4^-, $PF_2Cl_2^-$, and PF_3Cl^-. Because the primary dissociation process for $PF_2Cl_2^-$ is the loss of Cl^- anions, it is appropriate to compare the bond energy in $PF_2Cl_2^-$ with that in PCl_4^- rather than PF_4^-. The experimental and computational results for PCl_4^- and $PF_2Cl_2^-$ indicate that changing the equatorial ligands from chlorine to fluorine increases the bond strength by 5−10 kJ/mol. The substitution of equatorial Cl atoms with F atoms should increase the charge on the central P atom and increase the electrostatic attractions in the molecule. Indeed, the NBO charge on the P atom increases by 0.65 when F atoms replace the equatorial Cl atoms (see Table 5). The negative charge on the axial atoms becomes greater, by 0.05 electrons. Thus, the product of the P-atom and axial

Cl-atom charges almost doubles, from −0.46 to −0.91, which suggests that the Coulombic attractions in the breaking bond are larger in $PF_2Cl_2^-$. The slight increase in bond strength may also be due to less-repulsive interactions between lone pairs on the axial chloride and the equatorial fluorine ligands. In any case, the significant change in the equatorial ligands has a rather small effect on the axial bond strength.

In contrast, the P−Cl bond strength in PF_3Cl^- is weaker than the bond strength in $PF_2Cl_2^-$ by 34 kJ/mol (experimental) or 26−39 kJ/mol (calculated). This comparison isolates a change in the axial halogen ligand *opposite* the bond that is breaking. The charge on the Cl atom is more negative in PF_3Cl^- than in $PF_2Cl_2^-$ (−0.80 versus −0.63). The weaker bond, longer bond length, and more negative charge are consistent with viewing PF_3Cl^- as a $PF_3{\cdot}Cl^-$ cluster. The calculated $F_{ax}-P-F_{eq}$ angles in PF_4^-, PF_3Cl^-, and PF_3 are 87.1°, 91.4°, and 97.4°. Thus, the PF_3 portion of PF_3Cl^- has a structure that is intermediate between those of PF_4^- and PF_3, in agreement with the cluster picture. A similar but weaker trend is observed in interhalogen hydrogen bond strengths, where $D(XH-Y^-)$ (where X and Y are halogens) is weaker for lighter halogens in the X position.[42] Hydrogen bonding can also be considered to be hypervalent bonding, because the central (H) atom nominally has two pairs of electrons in its valence shell.[7,43] In both cases, a stronger bond from the central atom to one halogen ligand has a tendency to monopolize the bonding orbital, which leaves the electrons on the other halogen in more nonbonding orbitals. Surprisingly, the opposite effect is seen in the trihalogen anions; the reasons for these opposing trends are under investigation.[44]

A different perspective on these bond strengths is provided by the "snap" bond energies, where the products are not allowed to rearrange to a lower energy geometry after dissociation.[45] The snap bond energies calculated at the B3LYP/aug-cc-pVTZ level (not corrected for zero-point energy, because the geometries are not optimized) are given in Table 3. The difference between the snap bond strength and the bond strength is the rearrangement energy. The rearrangement energy is 61 and 64 kJ/mol for the dissociation of PCl_4^- and $PF_2Cl_2^-$, respectively, but only 21 kJ/mol for PF_3Cl^-. The bond in $PF_2Cl_2^-$ is slightly stronger than the bond in PCl_4^-, regardless of whether the products are allowed to optimize their geometry. The much smaller rearrangement energy in PF_3Cl^-, as well as a snap bond energy that is only half that of $PF_2Cl_2^-$, are consistent with the $PF_3{\cdot}Cl^-$ cluster description.

Comparison of PCl_4^- and $POCl_4^-$. The measured bond strength in $POCl_4^-$ is only about half that in PCl_4^-. The substantial experimental weakening of 47 kJ/mol is actually smaller than the computational difference (57−71 kJ/mol). However, the difference in bond strengths is not reflected in the computed geometries for these ions. For both, two Cl atoms are in axial positions, and two Cl atoms are in equatorial positions. The calculated axial bond lengths in these molecules are almost the same, and the calculated equatorial bond length is actually shorter in $POCl_4^-$.

The snap bond energies are $D_{snap}(PCl_3-Cl^-) = 158$ kJ/mol and $D_{snap}(POCl_3-Cl^-) = 222$ kJ/mol. Thus, formally adding an O atom to PCl_4^- to make $POCl_4^-$ increases the P−Cl$^-$ snap bond strength. The rearrangement energy is 61 kJ/mol for PCl_3 and 182 kJ/mol for $POCl_3$. The $POCl_3-Cl^-$ bond is not intrinsically weak; rather, the $POCl_3$ moiety strongly prefers a pseudo-tetrahedral geometry (whereas the preference of PCl_3 for a pyramidal geometry is substantially less).

Comparison of $POCl_4^-$ and $PSCl_4^-$. Substitution of a S atom for the O atom in $POCl_4^-$ gives a further test of how changing the electronegativity of an equatorial ligand affects the strength of a hypervalent bond. The experimental results show a negligible decrease (2 kJ/mol) in the experimental bond strength. The computational results show that the bond strength decreases by 7−9 kJ/mol, except for the G2(MP2) method, which gives a bond strength increase of 17 kJ/mol. As observed in the comparison of PCl_4^- to $PF_2Cl_2^-$, the experimental results and the computational methods—except G2(MP2)—indicate that more-electronegative equatorial ligands increase the bond strengths in hypervalent systems, whereas the G2(MP2) method gives the opposite trend. G2-type methods are primarily optimized for lighter elements and can have difficulties for phosphorus- and sulfur-containing molecules.[46]

The snap bond strength $D_{snap}(PSCl_3-Cl^-)$ is calculated to be 190 kJ/mol, which is exactly between $D_{snap}(PCl_3-Cl^-) = 158$ kJ/mol and $D_{snap}(POCl_3-Cl^-) = 222$ kJ/mol. Thus, the addition of a sulfur ligand increases the P−Cl$^-$ snap bond energy less than an oxygen ligand; however, the effect is canceled almost exactly by the differences in the rearrangement energy. Comparison of the NBO charges shows that sulfur is much less negatively charged than the O atom (−0.43 versus −1.01). This difference is mostly balanced by changes in the P-atom charge (0.86 in $PSCl_4^-$ and 1.49 in $POCl_4^-$). Electrostatic effects may account for the differences in the snap bond strengths in $PECl_4^-$ systems.

Comparison of $POCl_4^-$ and POF_4^-. Larson and McMahon reported that the addition of an O atom to PX_4^- strengthens the P−F$^-$ bond by 32 kJ/mol, whereas the computed effect is in the range of 34−42 kJ/mol. This result is contrary to the substantial weakening of the P−Cl$^-$ bond that is observed when oxygen is added to PCl_4^-, so different factors must be dominant in the fluorinated system. The geometry changes that occur upon the addition of oxygen are similar for the PCl_4^- and PF_3^- systems. The rearrangement energy after breaking a POF_3-F^- bond (208 kJ/mol) is somewhat larger than that for a $POCl_3-Cl^-$ bond (182 kJ/mol); this is consistent with larger force constants for bending P−F bonds away from their preferred geometry. The snap bond energy $D_{snap}(POF_3-F^-) = 441$ kJ/mol is sufficiently large that even a substantial rearrangement energy is not sufficient to make the POF_3-F^- bond weaker than the PF_3-F^- bond.

Conclusions

The P−Cl$^-$ bond strengths in $PF_2Cl_2^-$, $POCl_4^-$, and $PSCl_4^-$ have been measured, and the results are in the range of 41−99 kJ/mol. The differences can be primarily attributed to the rearrangement energies of the dissociation products. The effects of rearrangement energies make periodic trends in the thermochemistry difficult to predict. Computational results give generally good agreement with the experimental values.

Acknowledgment. This material is based upon work supported by the National Science Foundation under Grant No. 9985883. We thank Peter Armentrout, Mary Rodgers, and Kent Ervin for use of the CRUNCH software for data analysis, the NIU Computational Chemistry Laboratory for computer usage, and the reviewers for insightful comments.

References and Notes

(1) Reed, A. E.; Schleyer, P. v. R. *J. Am. Chem. Soc*. **1990**, *112*, 1434−1445.

(2) Norman, N. C. *Periodicity and the P-block Elements*; Oxford University Press: Oxford, U.K., 1994.

(3) Magnusson, E. *J. Am. Chem. Soc*. **1990**, *112*, 7940−7951.

(4) Noury, S.; Silvi, B.; Gillespie, R. J. *Inorg. Chem.* **2002**, *41*, 2164−2172.

(5) Gillespie, R. J.; Silvi, B. *Coord. Chem. Rev.* **2002**, *233*−*234*, 53−62.

(6) Molina, J. M.; Dobado, J. A. *Theor. Chem. Acc.* **2001**, *105*, 328−337.

(7) Landrum, G. A.; Goldberg, N.; Hoffmann, R. *J. Chem. Soc., Dalton Trans.* **1997**, 3605−3613.

(8) Kaupp, M.; van Wüllen, Ch.; Franke, R.; Schmitz, F.; Kutzelnigg, W. *J. Am. Chem. Soc.* **1996**, *118*, 11939−11950.

(9) Larson, J. W.; McMahon, T. B. *J. Am. Chem. Soc.* **1983**, *105*, 2944−2950. Larsen, J. W.; McMahon, T. B. *J. Am. Chem. Soc.* **1985**, *107*, 766−775.

(10) Walker, B. W.; Check, C. E.; Lobring, K. C.; Pommerening, C. A.; Sunderlin, L. S. *J. Am. Soc. Mass Spectrom.* **2002**, *13*, 469−476.

(11) Heil, T. E.; Check, C. E.; Lobring, K. C.; Sunderlin, L. S. *J. Phys. Chem. A* **2002**, *106*, 10043−10048.

(12) Sunderlin, L. S. Hypervalent Bonding in Gas-Phase Anions. In *Advances in Gas-Phase Ion Chemistry*; Adams, N., Babcock, L., Eds.; JAI Press: Greenwich, CT, 2001; Vol. 4.

(13) Larson, J. W.; McMahon, T. B. *Inorg. Chem.* **1987**, *36*, 4018−4023.

(14) Bogdanov, B.; Peschke, M.; Tonner, D. S.; Szulejko, J. E.; McMahon, T. B. *Int. J. Mass Spectrom.* **1999**, *185*, 707−725.

(15) Wenthold, P. G.; Squires, R. R. *J. Phys. Chem.* **1995**, *99*, 2002−2005.

(16) Lobring, K. C.; Check, C. E.; Sunderlin, L. S. *Int. J. Mass Spectrom.* **2003**, *222*, 221−227.

(17) Christe, K. O.; Dixon, D. A.; Schrobilgen, G. J.; Wilson, W. W. *J. Am. Chem. Soc.* **1997**, *119*, 3918−3928.

(18) Lugez, C. L.; Irikura, K. K.; Jacox, M. E. *J. Chem. Phys.* **1998**, *108*, 8381−8393.

(19) Reed, A. E.; Schleyer, P. v. R. *J. Am. Chem. Soc.* **1990**, *112*, 1434−1445.

(20) Dobado, J. A.; Martínez-García, H.; Molina, J. M.; Sundberg, M. R. **1998**, *120*, 8461−8471.

(21) Chesnut, D. B.; Savin, A. *J. Am. Chem. Soc.* **1999**, *121*, 2335−2336.

(22) Yang, C.; Goldstein, E.; Breffle, S.; Jin, S. *J. Mol. Struct.* **1992**, *259*, 345−368.

(23) Muntean, F.; Armentrout, P. B. *J. Chem. Phys.* **2001**, *115*, 1213−1228 and references therein.

(24) Armentrout, P. B. *J. Am. Soc. Mass Spectrom.* **2002**, *13*, 419−434.

(25) Do, K.; Klein, T. P.; Pommerening, C. A.; Sunderlin, L. S. *J. Am. Soc. Mass Spectrom.* **1997**, *8*, 688−696.

(26) Williamson, D. H.; Mayhew, C. A.; Knighton, W. B.; Grimsrud, E. P. *J. Chem. Phys.* **2000**, *113*, 11035−11043.

(27) Ervin, K. M.; Armentrout, P. B. *J. Chem. Phys.* **1985**, *83*, 166−189. Rodgers, M. T.; Ervin, K. M.; Armentrout, P. B. *J. Chem. Phys.* **1997**, *106*, 4499−4508.

(28) Nakamoto, K. *Infrared and Raman Spectra of Inorganic and Coordination Compounds Part A: Theory and Applications in Inorganic Chemistry*, 5th ed. Wiley: New York, 1997.

(29) Ahlijah, G. Y.; Goldstein, M. *J. Chem. Soc. A* **1970**, 326−329. Ahlijah, G. Y.; Goldstein, M. *Chem. Commun.* **1968**, 1356−1358.

(30) Gurvich, L. V.; Veyts, I. V.; Alcock, C. B. *Thermochemical Properties of Individual Substances*, 4th ed.; Hemisphere Publishing: New York, 1989.

(31) Check, C. E.; Faust, T. O.; Bailey, J. E.; Wright, B. J.; Gilbert, T. M.; Sunderlin, L. S. *J. Phys. Chem. A* **2001**, *105*, 8111−8116.

(32) Robertson, E. G.; McNaughton, D. *J. Phys. Chem. A* **2003**, *107*, 642−650.

(33) Loh, S. K.; Hales, D. A.; Lian, L.; Armentrout, P. B. *J. Chem. Phys.* **1989**, *90*, 5466−5485. Schultz, R. H.; Crellin, K. C.; Armentrout, P. B. *J. Am. Chem. Soc.* **1991**, *113*, 8590−8601.

(34) Frisch, M. J.; Trucks, G. W.; Schlegel, H. B.; Scuseria, G. E.; Robb, M. A.; Cheeseman, J. R.; Zakrzewski, V. G.; Montgomery, J. A., Jr.; Stratmann, R. E.; Burant, J. C.; Dapprich, S.; Millam, J. M.; Daniels, A. D.; Kudin, K. N.; Strain, M. C.; Farkas, O.; Tomasi, J.; Barone, V.; Cossi, M.; Cammi, R.; Mennucci, B.; Pomelli, C.; Adamo, C.; Clifford, S.; Ochterski, J.; Petersson, G. A.; Ayala, P. Y.; Cui, Q.; Morokuma, K.; Malick, D. K.; Rabuck, A. D.; Raghavachari, K.; Foresman, J. B.; Cioslowski, J.; Ortiz, J. V.; Stefanov, B. B.; Liu, G.; Liashenko, A.; Piskorz, P.; Komaromi, I.; Gomperts, R.; Martin, R. L.; Fox, D. J.; Keith, T.; Al-Laham, M. A.; Peng, C. Y.; Nanayakkara, A.; Gonzalez, C.; Challacombe, M.; Gill, P. M. W.; Johnson, B. G.; Chen, W.; Wong, M. W.; Andres, J. L.; Head-Gordon, M.; Replogle, E. S.; Pople, J. A. *Gaussian 98*, revision A.9; Gaussian, Inc.: Pittsburgh, PA, 1998.

(35) Glendening, E. D.; Badenhoop, J. K.; Reed, A. E.; Carpenter, J. E.; Bohmann, J. A.; Morales, C. M.; Weinhold, F. NBO Version 5.0; Theoretical Chemistry Institute, University of Wisconsin, Madison, WI, 2001. (http://www.chem.wisc.edu/∼nbo5.)

(36) Wiberg, N. *Holleman−Wiberg Inorganic Chemistry*, 1st English ed. Academic Press: San Diego, CA, 2001.

(37) Mingos, D. M. P. *Essential Trends in Inorganic Chemistry*. Oxford University Press: Oxford, U.K., 1998.

(38) Macho, C.; Minkwitz, R.; Rohmann, J.; Steger, B.; Wölfel, V.; Oberhammer, H. *Inorg. Chem.* **1986**, *25*, 2828−2835.

(39) Robinson, E. A.; Gillespie, R. J. *Inorg. Chem.* **2003**, *42*, 3865−3872.

(40) Mauksch, M.; Schleyer, P. v. R. *Inorg. Chem.* **2001**, *40*, 1756−1769.

(41) Hay, P. J.; Wadt, W. R. *J. Chem. Phys.* **1985**, *82*, 270−283. Wadt, W. R.; Hay, P. J. *J. Chem. Phys.* **1985**, *82*, 284−298. Hay, P. J.; Wadt, W. R. *J. Chem. Phys.* **1985**, *82*, 299−310.

(42) Larson, J. W.; McMahon, T. B. *Inorg. Chem.* **1984**, *23*, 2029−2033. Caldwell, G.; Kebarle, P. *Can. J. Chem.* **1985**, *63*, 1399−1406.

(43) Pimentel, G. C. *J. Chem. Phys.* **1951**, *19*, 446−448.

(44) Check, C. E.; Lobring, K. C.; Hao, C.; Wright, B. J.; Banweg, N.; Ivanov, M. R. J.; White, E.; Bailey, J. M.; Gilbert, T. M.; Sunderlin, L. S., manuscript in preparation.

(45) More sophisticated approaches to this issue are exemplified by the method of "Intrinsic Bond Energies." (Grimme, S. *J. Am. Chem. Soc.* **1996**, *118*, 1529−1534. Exner, K.; Schleyer, P. v. R. *J. Phys. Chem. A* **1991**, *105*, 3407−3416.) However, such techniques are not well parametrized for phosphorus−halogen bonds.

(46) Curtiss, L. A.; Raghavachari, K.; Redfern, P. C.; Rassolov, V.; Pople, J. A. *J. Chem. Phys.* **1998**, *109*, 7764−7776.

(47) Morino, Y.; Kuchitsu, K.; Moritani, T. *Inorg. Chem.* **1969**, *8*, 867−871.

(48) Kawashima, Y.; Cox, A. P. *J. Mol. Spectrosc.* **1977**, *65*, 319−329.

(49) Brittain, A. H.; Smith, J. E.; Schwendeman, R. H. *Inorg. Chem.* **1972**, *11*, 39−42.

(50) Hedberg, K.; Iwasaki, M. *J. Chem. Phys.* **1962**, *36*, 589−594.

(51) Kisliuk, P.; Townes, C. H. *J. Chem. Phys.* **1950**, *18*, 1109−1111.

(52) Williams, Q.; Sheridan, J.; Gordy, W. *J. Chem. Phys.* **1952**, *20*, 164−167.

(53) Firth, S.; Davis, R. W. *J. Mol. Spectrosc.* **1988**, *127*, 209−221.